

# NONLINEAR STOCHASTIC BIASING OF GALAXIES AND DARK HALOS IN COSMOLOGICAL HYDRODYNAMIC SIMULATIONS

Kohji Yoshikawa

*Department of Astronomy, Kyoto University, Kyoto 606-8502, Japan.*

kohji@kusastro.kyoto-u.ac.jp

Atsushi Taruya

*Department of Physics, School of Science, University of Tokyo, Tokyo 113-0033, Japan.*

ataruya@utap.phys.s.u-tokyo.ac.jp

Y.P. Jing

*Shanghai Astronomical Observatory, the Partner Group of MPI für Astrophysik,  
Nandan Road 80, 200030 Shanghai, China.*

*and*

*National Astronomical Observatories, Chinese Academy of Sciences, 100012 Beijing, China.*

ypjing@center.shao.ac.cn

*and*

Yasushi Suto

*Department of Physics and Research Center for the Early Universe (RESCEU)  
School of Science, University of Tokyo, Tokyo 113-0033, Japan.*

suto@phys.s.u-tokyo.ac.jp

## ABSTRACT

We perform an extensive analysis of nonlinear and stochastic biasing of galaxies and dark halos in spatially flat low-density CDM universe ( $\Omega_0 = 0.3$ ,  $\lambda_0 = 0.7$ ,  $h = 0.7$ , and  $\sigma_8 = 1$ ) using cosmological hydrodynamic simulations. We identify galaxies by linking cold and dense gas particles which satisfy the Jeans criterion. We compare their biasing properties with the predictions of an analytic halo biasing model. Dark halos in our simulations exhibit reasonable agreement with the predictions only on scales larger than  $\sim 10h^{-1}\text{Mpc}$ , and on smaller scales the volume exclusion effect of halos due to their finite size becomes substantial. Interestingly the biasing properties of galaxies are better described by *extrapolating* the halo biasing model predictions.

The clustering amplitudes of galaxies are almost independent of the redshift between  $z = 0$  and  $3$  as reported in previous simulations. This in turn leads to a rapidly evolving biasing factor; we find that  $b_{\text{cov}} \simeq 1$  at redshift  $z \simeq 0$  to  $b_{\text{cov}} \simeq 3 - 4$  at  $z = 3$ , where  $b_{\text{cov}}$  is a biasing parameter defined from the linear regression of galaxy and dark matter density fields. Those values are consistent with the observed clustering of Lyman-break galaxies.

We also find the clear dependence of galaxy biasing on their formation epoch; the distribution of old populations of galaxies tightly correlates with the underlying mass density field, while that of young populations is slightly more stochastic and anti-biased relative to dark matter. The amplitude of two-point correlation function of old populations is about 3 times larger than that of the young populations. Furthermore, the old population of galaxies reside within massive dark halos while the young galaxies are preferentially formed in smaller dark halos. Assuming that the observed early and late-type galaxies correspond to the simulated old and young populations of galaxies, respectively, all of these segregations of galaxies are consistent with observational ones for the early and late-type of galaxies such as the morphology–density relation of galaxies.

*Subject headings:* galaxies: clustering – galaxies: formation – galaxies: halos – dark matter – cosmology: large-scale structure of universe – methods: numerical

## 1. INTRODUCTION

Ongoing galaxy redshift surveys, such as the Sloan Digital Sky Survey (SDSS) and the Two-Degree Field (2dF), aim at revealing the the large-scale structure of the universe with unprecedented precision. The gravitational instability is the main key process of the *dark matter clustering*, and this is now well understood from numerical simulations and several empirical theoretical models (Davis et al. 1985; Hamilton et al. 1991; Suto 1993; Mo & White 1996; Navarro, Frenk & White 1997). In fact once the underlying cosmological models are specified, the two-point correlation functions of dark matter, which are the most conventional and widely used statistics describing the large-scale structure, can be fairly accurately predicted even with the redshift distortion and light-cone effects (Peacock & Dodds 1996; Suto et al. 1999; Suto, Magira, & Yamamoto 2000; Hamana, Colombi, & Suto 2001).

On the other hand, it is widely believed that the distribution of galaxies is somewhat biased with respect to the underlying dark matter. For instance, Lyman-break galaxies at redshift  $z \approx 3$  (Steidel et al. 1998; Adelberger et al. 1998; Giavalisco et al. 1998) exhibit strong clustering and the galaxy biasing with respect to dark matter is time-dependent. Also the galaxy clustering is dependent on the galaxy morphology and environment (Dressler 1980; Postman & Gellar 1984; Loveday et al. 1995; Hermit et al. 1996; Dressler et al. 1997; Tegmark & Bromley 1999) indicating the galaxy biasing is sensitive to many physical processes and thus *stochastic*. Clearly the rela-

tion between galaxy and dark matter clustering is far from simple and not yet fully understood either observationally or theoretically. This is the primary difficulty in properly interpreting the observational data of the upcoming large-scale redshift surveys.

So far several models of galaxy biasing have been proposed adopting simplifying assumptions; Fry (1996) and Tegmark & Peebles (1998) discuss the evolution of biasing assuming that the number of galaxies does not change. Mo & White (1996) present a model for the nonlinear biasing of virialized dark halos using the extended Press–Schechter formalism (Bond et al. 1991). Jing (1998) tested and improved the formula for the biasing of halo correlation functions originally proposed by Mo & White (1996) using high-resolution  $N$ -body simulations. Dekel & Lahav (1999) develop a fundamental framework to quantify the nonlinearity and stochasticity in galaxy biasing. Their formulation was subsequently applied to several numerical simulations (Blanton et al. 1999, 2000; Somerville et al. 2001). The biasing of dark halos is also investigated by Kravtsov & Klypin (1999) using high resolution  $N$ -body simulations. Note that their definition of dark *halos* is different from the conventional one used in the Press–Schechter formalism but rather close to *dark matter cores* (DM cores) in our analysis below. Recently, Taruya & Suto (2000; TS hereafter) proposed a first physical and analytical model for nonlinear and stochastic halo biasing combining the biasing model of Mo & White (1996) and the formation epoch distribution (Kitayama & Suto 1996).

More realistic approaches to galaxy biasing employ the state-of-the-art numerical simulations including the mesh-based hydrodynamical simulations (Blanton et al. 1999, 2000; Cen & Ostriker 2000), and  $N$ -body simulations combined with semi-analytic modeling of galaxy formation (Benson et al. 2000; Somerville et al. 2001). In what follows, we use the cosmological smoothed particle hydrodynamic (SPH) simulations (Yoshikawa, Jing & Suto 2000) of cold dark matter (CDM) universe to examine the galaxy biasing. In particular, we focus on the comparison of the biasing characteristics of simulated objects (galaxies and dark halos) with the halo biasing model of TS. In addition, we investigate dependence of galaxy biasing properties on their formation history as an origin of galaxy morphology. Our simulation directly follows hydrodynamical and radiative processes to simulate galaxy formation, while the evolution of galaxies is not so properly modeled as those combined with a semi-analytic method of galaxy formation (Somerville et al. 2001). Due to the Lagrangian nature of the SPH technique, the spatial resolution of our simulations is better than those in the mesh-hydro simulations by Blanton et al. (1999, 2000) and we can resolve galaxies as distinct and isolated objects, while their treatment of the thermal process and the metal enrichment is more realistic. Thus our method is complementary to those previous investigations with different approaches.

The rest of the paper is organized as follows. In §2, we describe the detail of our numerical simulation and the procedures to identify galaxies, dark matter cores (DM cores), and dark halos. In §3 we present a brief summary of the biasing description following TS, and compare several properties of the biasing in the one-point statistics of galaxies and dark halos. Then we discuss the biasing in terms of their two-point correlation functions. Section 4 examines the dependence of galaxy biasing on their formation history. Finally, we summarize our major findings in §5.

## 2. METHODOLOGY

### 2.1. Cosmological SPH simulation

Our numerical simulation code is a hybrid of Particle–Particle–Particle–Mesh (P<sup>3</sup>M)  $N$ -body Poisson solver (Hockney & Eastwood 1981) and smoothed particle hydrodynamics (SPH) algorithm (Yoshikawa, Jing & Suto 2000). The simulation presented in this paper adopts  $N_{\text{DM}} = 128^3$  dark matter particles and the same number of gas particles for SPH. We use the spline (S2) functional form for gravitational softening (Hockney & Eastwood 1981) and the softening length is set to  $\epsilon_{\text{grav}} = L_{\text{box}}/(10N_{\text{DM}}^{1/3})$  and kept constant in comoving coordinates, where  $L_{\text{box}}$  is the comoving size of the simulation box. We set the minimum of SPH smoothing length to  $h_{\text{min}} = \epsilon_{\text{grav}}/4$  and adopt the ideal gas equation of state with an adiabatic index  $\gamma = 5/3$ . The effect of radiative cooling is included adopting the metallicity of  $[\text{Fe}/\text{H}] = -0.5$ . We use the cooling rate described in Sutherland & Dopita (1993). Thacker et al. (2000) reported that artificial over-cooling occurs under the presence of radiative cooling in SPH simulations due to overestimate of hot gas density in the vicinity of cooled gas clumps due to the smoothing scheme of SPH algorithm. In order to avoid this numerical artifact, we implement a modification of SPH algorithm, “cold gas decoupling”, following Pearce et al. (1999). The detail of this prescription is presented in the next subsection.

We consider a spatially-flat low-density CDM (LCDM) universe with  $\Omega_0 = 0.3$ ,  $\lambda_0 = 0.7$ ,  $\sigma_8 = 1.0$  and  $h = 0.7$ , where  $\Omega_0$  is the mean mass density parameter,  $\lambda_0$  the dimensionless cosmological constant,  $\sigma_8$  the rms density fluctuation on a scale of  $8h^{-1}$  Mpc and  $h$  the Hubble constant in units of  $100 \text{ km}\cdot\text{s}^{-1}\cdot\text{Mpc}^{-1}$ . This particular model satisfies both the *COBE* normalization (Bunn & White 1997) and the abundance of X-ray clusters of galaxies (Kitayama & Suto 1997). We assume the mean baryon mass density parameter to be  $\Omega_b = 0.015h^{-2}$  (Copi et al. 1995). The simulation is carried out in a periodic cube of  $(75h^{-1}\text{Mpc})^3$ , with the gas and dark matter mass per particle being  $2.4 \times 10^9 M_\odot$  and  $2.2 \times 10^{10} M_\odot$ , respectively. The initial condition is created at  $z = 25$  using the COSMICS package (Bertschinger 1995), which is evolved up to  $z = 0$ .

### 2.2. Cold gas decoupling and identification of galaxies

In order to avoid the numerical over-cooling of gas particles mentioned above, we decouple cold gas particles which satisfy the following Jeans condition (Yoshikawa, Jing & Suto 2000):

$$h_{\text{SPH}} > \frac{c_s}{\sqrt{\pi G \rho_{\text{gas}}}}, \quad (1)$$

where  $h_{\text{SPH}}$  is the smoothing length of gas particles,  $c_s$  the sound speed,  $G$  the gravitational constant and  $\rho_{\text{gas}}$  the gas density of gas particles. Except for the fact that these cold gas particles are ignored in computing the gas density of hot gas particles, all the other SPH interactions are left unchanged. This decoupling scheme is a phenomenological treatment of multi-phase gas dynamics, and should be interpreted as an approximate prescription of galaxy formation.

Galaxies in our simulations are identified as clumps of cold and dense gas particles which satisfy the criterion (1) and

$$\rho_{\text{gas}} > 10^2 \bar{\rho}_{\text{b}}(z), \quad (2)$$

where  $\bar{\rho}_{\text{b}}(z)$  is the mean baryon density at redshift  $z$ . Figure 1 shows the scatter plots of gas particles in density – temperature plane. The blue points indicate the cold and dense gas particles satisfying the criteria (1) and (2), the diffuse cold gas particles which satisfy (1) and  $\rho_{\text{gas}} < 10^2 \bar{\rho}_{\text{b}}(z)$  are plotted in green, and the other hot gas particles are represented in red. This indicates that the above criteria for the galaxy particles properly segregate the cold and dense gas particles. We group these particles using friend-of-friend (FOF) algorithm (Davis et al. 1985) with linking length  $b_{\text{g}} = 0.0164(1+z)\bar{l}$  and identify the resulting clumps as “galaxies”, where  $\bar{l} = L_{\text{box}}/N_{\text{DM}}^{1/3}$  is the comoving mean particle separation. The proper choice of the linking length is not clear and we simply adopt the value of Pearce et al. (1999) here. In this paper, we only consider galaxies with mass greater than  $M_{\text{g,min}} = 10^{11} M_{\odot}$ , which is equivalently 40 times of each gas particle mass and close to a nominal mass resolution of baryonic matter<sup>1</sup>. As noted in § 2.3, the mass functions of simulated galaxies are roughly consistent with those from semi-analytic modeling of galaxy formation, which justifies our galaxy criteria empirically to some extent. We show the number of galaxies identified in our simulation and the adopted linking length in Table 1.

### 2.3. Identification of dark halos and dark matter cores

The FOF algorithm is also applied in identifying dark halos. The linking length  $b_{\text{h}}$  for dark halos is set to satisfy the equation

$$\frac{\Delta_{\text{c}}(z)}{18\pi^2} = \left( \frac{b_{\text{h}}}{0.2\bar{l}} \right)^{-3}, \quad (3)$$

where  $\Delta_{\text{c}}(z)$  is the mean over-density of spherically virialized objects formed at redshift  $z$ . We compute  $\Delta_{\text{c}}(z)$  at each redshift using a fitting formula by Kitayama & Suto (1996). At  $z = 0$ , for instance,  $\Delta_{\text{c}} = 335$  and  $b_{\text{h}} = 0.164\bar{l}$ .

We also identify the surviving high-density substructures in dark halos, which we call DM cores. Identification of substructures in dark halos is a technically challenging problem and several objective methods have been proposed so far (Gelb & Bertschinger 1994; Eisenstein & Hut 1998; Klypin et al. 1999; Springel et al. 2000). In order to identify DM cores in our simulation, we adopt the hierarchical FOF (HFOF) method (Gottlöber et al. 1999). In HFOF method, we apply the conventional FOF method with a set of different linking length  $b_{\text{c}}$ :  $b_{\text{c}} = l_{\text{max}}/4$ ,  $l_{\text{max}}/2$ , and  $l_{\text{max}}$ , where  $l_{\text{max}}$  is the maximum linking length. For each linking length, gravitationally bound groups with more than 20 particles are identified as DM cores. The maximum linking length is set to  $l_{\text{max}} = 0.05\bar{l}$ .

---

<sup>1</sup>SPH gas density is smoothed over about 30 nearest neighbor gas particles.

In this paper, we consider the dark halos with their mass greater than  $10^{12}M_{\odot}$  ( $\simeq \Omega_0/\Omega_b \times M_{g,\min}$ ) and DM cores with more than 20 dark matter particles (equivalently  $4.3 \times 10^{11}M_{\odot}$ ). In Table 1, the number of identified objects and adopted linking length are also shown. Figures 2 and 3 show the distribution of dark matter particles, gas particles, dark halos and galaxies at  $z = 0$  and  $z = 2$ . At  $z = 0$  galaxies are more strongly clustered than dark halos, while at  $z = 2$  those two objects show similar spatial distribution.

Figures 4 and 5 show close-up snapshots of the most massive cluster at  $z = 0$  with mass  $M \simeq 8 \times 10^{14}M_{\odot}$  and a relatively poor cluster with  $M \simeq 10^{14}M_{\odot}$ , respectively. In each figure, upper panels depict the distribution of dark matter and gas particles, and the distributions of DM cores and dense cold gas particles which satisfy the condition (1) and (2) are shown in lower panels. Circles in lower panels indicate the positions of galaxies identified in our simulation. We can see that for the richer cluster, the distribution of DM cores is relatively in good agreement with that of galaxies except for the cluster center, where the tidal radius is much shorter than our numerical resolution. On the other hand, galaxies or cold gas clumps in the smaller cluster are not necessarily hosted by DM cores. This is probably because DM cores in our simulation significantly suffer from the artificial overmerging, which is severer for poorer dark halos due to small number of particles, while galaxies represented by dissipative gas particles are less affected by this overmerging. This is why DM cores at higher redshift are much less abundant than galaxies and dark halos (see Table 1). This problem is intrinsically related to the question of whether substructures within dark halos identified in high-resolution  $N$ -body simulations (Klypin et al. 1999; Colín et al. 1999) really correspond to the real galaxies. Unfortunately the resolution of our current simulations is not sufficiently good to answer this issue in a reliably manner, but we hope to revisit this with another SPH run with  $N = 256^3$  particles (Yoshikawa, Jing & Suto, in preparation).

Figure 6 shows mass function of dark halos and galaxies at  $z = 0$  and 2. We find that the mass function of simulated dark halos (*upper panels*) agrees better to the fitting formula of Jenkins et al. (2001) (*dashed lines*) than that of Press & Schechter (1974) (*solid lines*). Galaxy mass functions in our simulations (*lower panels*) are roughly consistent with those from other SPH simulations and semi-analytic models (Benson et al. 2001), but slightly less abundant at  $M_{\text{galaxy}} \lesssim 10^{11}M_{\odot}$  due to limited mass resolution.

### 3. BIASING PROPERTIES OF GALAXIES AND DARK HALOS

The most natural form of galaxy biasing is the relation between over-density fields of galaxies  $\delta_g$  and dark matter  $\delta_m$ . In this section, we compute the density fields of galaxies and dark halos from our simulation, and study their statistical properties and evolution.

### 3.1. Formulation and computation of biasing parameters

A biasing scheme relates the density field of dark matter with those of galaxies and dark halos, which are defined for a given smoothing scale  $R_s$  as

$$\delta_m(\mathbf{x}, R_s) = \frac{\rho(\mathbf{x}, R_s)}{\bar{\rho}} - 1, \quad (4)$$

$$\delta_g(\mathbf{x}, R_s) = \frac{n_g(\mathbf{x}, R_s)}{\bar{n}_g} - 1, \quad (5)$$

$$\delta_h(\mathbf{x}, R_s) = \frac{n_h(\mathbf{x}, R_s)}{\bar{n}_h} - 1, \quad (6)$$

where  $\rho(\mathbf{x}, R_s)$ ,  $n_g(\mathbf{x}, R_s)$ , and  $n_h(\mathbf{x}, R_s)$  denote the mass density, and galaxy and halo number densities smoothed over the top-hat window radius  $R_s$ , and the over-bar ( $\bar{\phantom{x}}$ ) indicates the mean over the entire universe. We briefly summarize several parameters describing the nonlinear stochastic nature of biasing introduced by TS for later convenience.

The joint probability distribution function (PDF),  $P(\delta_m, \delta_i)$ , characterizes the statistical properties of  $\delta_m$  and  $\delta_i$ , where the subscript  $i$  indicates two different objects; “g” for galaxies and “h” for dark halos. By definition,  $\delta_m$  and  $\delta_i$  have zero mean and their variances are related to the joint PDF as

$$\sigma_m^2 = \langle \delta_m^2 \rangle = \int \int P(\delta_m, \delta_i) \delta_m^2 d\delta_m d\delta_i \quad (7)$$

and

$$\sigma_i^2 = \langle \delta_i^2 \rangle = \int \int P(\delta_m, \delta_i) \delta_i^2 d\delta_m d\delta_i, \quad (8)$$

where the bracket  $\langle \dots \rangle$  denotes the joint average over  $\delta_i$  and  $\delta_m$ . The statistical relation between  $\delta_i$  and  $\delta_m$  is described by the conditional PDF,  $P(\delta_i|\delta_m)$ . The conditional mean of  $\delta_i$ ,  $\bar{\delta}_i(\delta_m)$ , for a given  $\delta_m$  is then calculated from

$$\bar{\delta}_i(\delta_m) = \int \delta_i P(\delta_i|\delta_m) d\delta_i, \quad (9)$$

yielding the following biasing parameter (TS):

$$b_{\text{cov},i} \equiv \frac{\langle \bar{\delta}_i(\delta_m) \delta_m \rangle}{\sigma_m^2} = \frac{\langle \delta_i \delta_m \rangle}{\sigma_m^2}. \quad (10)$$

The nonlinearity of the biasing is quantified by

$$\epsilon_{\text{nl},i}^2 \equiv \frac{\langle \delta_m^2 \rangle \langle \bar{\delta}_i^2 \rangle}{\langle \bar{\delta}_i \delta_m \rangle^2} - 1 = \frac{\sigma_m^2 \langle \bar{\delta}_i^2 \rangle}{\langle \delta_i \delta_m \rangle^2} - 1, \quad (11)$$

which vanishes only when the biasing is linear (i.e., the ratio  $\delta_i/\delta_m$  is independent of  $\delta_m$ ) and is positive otherwise. Similarly the stochasticity of the biasing is characterized by

$$\epsilon_{\text{scatt},i}^2 \equiv \frac{\langle \delta_m^2 \rangle \langle (\delta_i - \bar{\delta}_i)^2 \rangle}{\langle \bar{\delta}_i \delta_m \rangle^2} = \frac{\sigma_m^2 [\sigma_i^2 - \langle \bar{\delta}_i^2 \rangle]}{\langle \delta_i \delta_m \rangle^2}. \quad (12)$$

This parameter vanishes for the deterministic bias where  $\delta_i = \bar{\delta}_i(\delta_m)$ . In terms of the above biasing parameters, a somewhat more conventional biasing coefficient  $b_{\text{var},i} \equiv \sigma_i/\sigma_m$  is written as

$$b_{\text{var},i} = b_{\text{cov},i} (1 + \epsilon_{\text{nl},i}^2 + \epsilon_{\text{scatt},i}^2)^{1/2}. \quad (13)$$

Finally the correlation coefficient  $r_{\text{corr},i}$  (Dekel & Lahav 1999) is given by

$$r_{\text{corr},i} \equiv \frac{\langle \delta_i \delta_m \rangle}{\sigma_i \sigma_m} = \frac{1}{\sqrt{1 + \epsilon_{\text{scatt},i}^2 + \epsilon_{\text{nl},i}^2}}. \quad (14)$$

We compute the biasing parameters  $b_{\text{cov},i}$ ,  $b_{\text{var},i}$ ,  $\epsilon_{\text{nl},i}$ ,  $\epsilon_{\text{scatt},i}$  and  $r_{\text{corr},i}$  each for dark halos and galaxies with smoothing scales  $R = 4h^{-1}\text{Mpc}$ ,  $8h^{-1}\text{Mpc}$  and  $12h^{-1}\text{Mpc}$ . We obtain many pairs of the values  $(\delta_i(\mathbf{x}, R_s), \delta_m(\mathbf{x}, R_s))$  for randomly selected points  $\mathbf{x}$  in the simulation volume and evaluate the biasing parameters using equations (7) – (14) by replacing the joint averages  $\langle \dots \rangle$  with averages over all selected points. The number of randomly selected points is 1000 for the top-hat smoothing scale  $R_s = 12h^{-1}\text{Mpc}$ , 5000 for  $R_s = 8h^{-1}\text{Mpc}$  and 30000 for  $R_s = 4h^{-1}\text{Mpc}$ . Since our simulation volume is  $75h^{-1}\text{Mpc}$  per side, most of the selected sampling points are not fully independent. Nevertheless we decided to make over-sampling in evaluating the mean and the variance of the density fields. Thus our quoted error-bars below may rather correspond to those in a bootstrap resampling method.

### 3.2. Comparison of biasing of galaxies and dark halos

Figure 7 shows the joint distribution of  $\delta_h$  and  $\delta_g$  with mass density field  $\delta_m$  at redshift  $z = 0$ , 1 and 2 smoothed over  $R_s = 12h^{-1}\text{Mpc}$  (*Upper panels*) and  $4h^{-1}\text{Mpc}$  (*Lower panels*). We plot the conditional mean relation  $\bar{\delta}_i(\delta_m)$  from our simulation results (*solid lines*) and from the theoretical prediction of halo biasing by TS (*dashed lines*). In computing theoretical predictions, we adjust the range of dark halo mass as our simulated dark halos (Table 1).

Consider first the results for dark halos. For a given smoothing scale, the simulated halos exhibit positive biasing for relatively small  $\delta_m$  in agreement with the predictions. On the other hand, they tend to be underpopulated for large  $\delta_m$ , or *anti-biased*. This is mainly due to the exclusion effect of dark halos due to their finite volume size as previously discussed in Taruya et al. (2001) using purely N-body simulations. The theoretical model of TS does not take account of this effect, and thus the discrepancy between the predictions and the simulations becomes more substantial for smaller  $R_s$  and/or at lower  $z$  as expected.

Since our identified *galaxies* have smaller spatial extent than the halos, the exclusion effect is not so serious. This is clearly illustrated in lower panels in Figure 7. In fact they seem to show much better agreement with the TS predictions despite the fact that the models are formally valid only for dark halos defined according to the Press-Schechter manner.



A more careful look at the results for galaxies, however, reveals that  $\bar{\delta}_g(\delta_m)/\delta_m$  decreases slightly at larger  $\delta_m$  especially for smaller smoothing scale  $R_s = 4h^{-1}\text{Mpc}$ . While this tendency may be partially explained by their volume exclusion effect, their typical sizes seem to be sufficiently small to account for this. Rather, we consider two possible origins of this tendency. One is the suppression of galaxy formation at very high temperature and thus high density regions, as pointed out in Blanton et al. (1999, 2000). Figure 8 shows the dependence of galaxy overdensity on the surrounding gas temperature separately for galaxies with different formation redshifts (see §4 for details), and supports this interpretation; the ratio,  $(1 + \delta_g)/(1 + \delta_m)$ , is anti-correlated with the surrounding gas temperature. Comparing the left and right panels in Figure 8 indicates that the anti-correlation with gas temperature is much stronger for galaxies which form relatively late ( $z_f < 1.7$ ). On the other hand, those formed earlier show very weak, at most, anti-correlation, which is natural because they should have collapsed and formed much before the surrounding gas acquires the current high temperature. Another possibility is that there is an intrinsic difference in formation epoch of galaxies between over- and under-dense regions. Since, in hierarchical formation scenarios, objects in over-dense regions tend to form earlier than those in under-dense regions, it is expected that young galaxies with  $z_f < 1.7$  form relatively lower-dense thus low-temperature regions, which is also consistent with Figure 8. The similar analysis for DM cores will distinguish these two possibilities. Although we notice that the same correlation exists even for DM cores, we suspect that this is mainly due to the artificial overmerging effect as we discussed in §2.3., and will revisit this topic with another simulation with higher-resolution (Yoshikawa, Jing & Suto, in preparation).

Incidentally, in order to check the dependence of the simulated galaxy biasing on the lower mass limit of our criteria,  $M_{\text{galaxy}} > 10^{11}M_\odot$  (or equivalently  $N_{\text{gas}} > 40$ ), we construct another set of galaxy sample adopting higher mass cutoff  $N_{\text{gas}} > 80$ , and compare their biasing properties. We find that the joint probability distribution of  $\delta_m$  and  $\delta_g$  for the galaxy sample selected with  $N_{\text{gas}} > 80$  does not significantly change from those of the original galaxy sample.

### 3.3. Stochasticity and nonlinearity in biasing of galaxies and dark halos

The stochasticity and nonlinearity in galaxy and halo biasing are clearly identified in Figures 7. For more quantitative discussion, we plot in Figure 9 the evolution of their biasing parameters  $b_{\text{cov}}$ ,  $r_{\text{corr}}$ ,  $\epsilon_{\text{scatt}}$  and  $\epsilon_{\text{corr}}$  for three different smoothing radii.

Consider first  $b_{\text{cov}}$ . This biasing parameter exhibits strong time-dependence; the biasing is stronger in the past. This is consistent with analytic biasing models (Mo & White 1996; Taruya & Suto 2000), previous numerical simulations (Kravtsov & Klypin 1999; Somerville et al. 2001; Pearce et al. 1999) and in fact explains the recent observations of Lyman break galaxies (Giavalisco et al. 1998; Adelberger et al. 1998) using the halo biasing model (Mo & White 1996; Jing & Suto 1998). On the other hand, the scale-dependence of  $b_{\text{cov}}$  is very weak as in the case of the biasing parameter defined through the two-point correlation function (see the next subsection).

Both  $\epsilon_{\text{scatt}}$  and  $\epsilon_{\text{nl}}$  in our simulated catalogues are somewhat smaller than the TS prediction, but their qualitative behavior is consistent with the model; larger on small scales and almost independent of  $z$ . The biasing becomes linear and deterministic relation and also the volume exclusion is less effective for larger smoothing scales. The current degree of the stochasticity and nonlinearity does not hardly affect the amplitude of clustering (see eq.[13]), but the topology of the isodensity contours is sensitive to the nonlinearity even at this level (Hikage, Taruya & Suto 2001).

It is interesting to notice that the biasing parameters for galaxies show similar behavior and are closer to the predicted behavior. In addition, all biasing parameters for dark halos and galaxies behave very similarly at high redshifts  $z \simeq 2 - 3$ . This indicates that the spatial distribution of galaxies and dark halos are statistically similar, and can be understood by the fact that we have one-to-one correspondence between dark halos and galaxies at  $z \simeq 2 - 3$  as shown below.

Figure 9 also shows that the evolution of biasing is almost independent on the lower mass limit of the galaxies. This might be interpreted as our simulated galaxy sample is nearly complete for the present purpose.

Figure 10 shows the number of member galaxies which reside within the virial radius of their hosting dark halos (*upper panels*) and the distribution of their mass ratios (*lower panels*) at redshift  $z = 0, 2$  and  $3$ . Solid and dashed lines in lower panels indicate the cosmic mean baryon fraction  $\Omega_b/\Omega_0$  and resolution limit of galaxy mass ( $M_{\text{galaxy}} = 10^{11} M_{\odot}$ ), respectively. One can see that most dark halos at  $z = 3$  host only one galaxy, explicitly justifying the *empirical* assumption of one-to-one correspondence between dark halos and Lyman-break galaxies around  $z = 3$  in previous studies (Jing & Suto 1998; Steidel et al. 1998). The subsequent evolution of dark halos involves several merger processes, and thus dark halos at lower redshifts tend to host multiple member galaxies.

### 3.4. Biasing in terms of the two-point correlation function

The previous subsections discuss only the biasing parameters defined from the one-point statistics. In this subsection, we turn to a more conventional biasing parameter defined through the two-point statistics:

$$b_{\xi,i}(r) \equiv \sqrt{\frac{\xi_{ii}(r)}{\xi_{\text{mm}}(r)}}, \quad (15)$$

where  $\xi_{ii}(r)$  and  $\xi_{\text{mm}}(r)$  are two-point correlation functions of objects  $i$  and of dark matter, respectively. While the above biasing parameter is ill-defined where either  $\xi_{ii}(r)$  or  $\xi_{\text{mm}}(r)$  becomes negative, it is not the case at clustering scales of interest ( $< 10h^{-1}\text{Mpc}$ ). The relation of one-point and two-point biasing parameters is also investigated in detail by Taruya et al. (2001) for density peaks and dark halos.

Figure 11 shows two-point correlation functions of dark matter, galaxies, dark halos and DM

cores (*upper and middle panels*), and the profiles of biasing parameters  $b_\xi(r)$  for those objects (*lower panels*) at  $z = 0, 1$  and  $2$ . In the upper panels, we show the correlation functions of DM cores identified with two different maximum linking length;  $l_{\max} = 0.05$  as presented in § 2.3 and  $l_{\max} = b_h/2$ . Correlation functions of DM cores identified with  $l_{\max} = 0.05$  are similar to those of galaxies. On the other hand, those identified with  $l_{\max} = b_h/2$  exhibit much weaker correlation, and are rather similar to those of dark halos. This is due to the fact that HFOF algorithm with larger  $l_{\max}$  tends to pick up lower mass halos which are poorly resolved in our numerical resolution.

The correlation functions of galaxies are almost unchanged with redshift, and that of dark halos only slightly evolves between  $z = 0$  and  $2$ . By contrast, the amplitude of the dark matter correlation function evolves rapidly by factor of  $\sim 10$  from  $z = 2$  to  $z = 0$ . The biasing parameter  $b_{\xi,g}$  is larger at a higher redshift, for example,  $b_{\xi,g} \simeq 2\text{--}2.5$  at  $z = 2$ . These results are consistent with the numerical studies by Bagla (1998), Colín et al. (1999) and Pearce et al. (1999) and also qualitatively explains the clustering of Lyman-break galaxies (Giavalisco et al. 1998). The biasing parameter  $b_{\xi,h}$  for dark halos is systematically lower than that of galaxies and DM cores again due to the volume exclusion effect. At  $z = 0$ , galaxies and DM cores are slightly anti-biased relative to dark matter at  $r \simeq 1h^{-1}\text{Mpc}$ , which is also consistent with previous numerical simulations (Pearce et al. 1999; Colín et al. 1999; Benson et al. 2000; Somerville et al. 2001) and also with the observational results from the Las Campanas Redshift Survey (Jing, Mo & Börner 1998). In lower panels, we also plot the one-point biasing parameter  $b_{\text{var},i} \equiv \sigma_i/\sigma_m$  at  $r = R_s$  for comparison. In general we find that  $b_{\xi,i}$  is very close to  $b_{\text{var},i}$  at  $z \sim 0$ , but systematically lower than  $b_{\text{var},i}$  at higher redshifts.

#### 4. THE FORMATION EPOCH AS AN ORIGIN OF THE MORPHOLOGICAL TYPE OF GALAXIES

It is fairly established that there exists a certain correlation between the morphology of galaxies and their star formation history; early-type galaxies form via initial star bursts at high redshifts while late-type galaxies experience continuous and relatively mild star formation history (Roberts & Haynes 1994; Kennicutt 1998). This implies that the galaxy morphology is empirically related to its formation epoch. On the basis of this interpretation, one can examine the morphology-dependent clustering of galaxies by classifying our simulated galaxies according to their formation epoch.

We have fifty outputs of all simulation particles at different redshifts between  $z = 9$  and  $0$ . For each galaxy identified at  $z = 0$ , we define its formation redshift  $z_f$  by the epoch when half of its *cooled gas* particles satisfy the criteria (1) and (2). Roughly speaking,  $z_f$  corresponds to the median formation redshift of *stars* in the present-day galaxies. We divide all simulated galaxies at  $z = 0$  into two populations (the young population with  $z_f < 1.7$  and the old population with  $z_f > 1.7$ ) so as to approximate the observed number ratio of 3/1 for late-type and early-type galaxies (Loveday et al. 1995).

Figure 12 shows the joint probability distribution of  $\delta_m$  and  $\delta_g$  respectively for the old (*left panel*) and young (*right panel*) populations. They exhibit clear difference in their clustering properties. Their biasing parameters are  $\sigma_g = 1.73(1.06)$ ,  $b_{\text{var},g} = 1.51(0.93)$  and  $r_{\text{corr},g} = 0.95(0.88)$  for the old (young) population. These results qualitatively agree with Blanton et al. (1999), and Somerville et al. (2001) also showed a similar result that red galaxies are biased compared to the overall population and blue ones are anti-biased, where galaxies with color  $B - V > 0.8$  are defined as red galaxies and the remainder as blue ones. The dashed lines in both panels indicate the TS predictions of the mean biasing for dark halos restricting the formation epoch as  $z_f > 1.7$  and  $z_f < 1.7$ , respectively; the old population shows excellent agreement with the halo biasing prediction while the young population behaves rather differently. This indicates that early-type galaxies preferentially reside in the center of the massive halos almost in a one-to-one manner and that late-type galaxies avoid the dense environment, which is consistent with the observed morphology-density relation (Dressler 1980; Postman & Gellar 1984; Dressler et al. 1997).

This interpretation is directly confirmed in Figure 13. Massive halos have a larger fraction of the old population of galaxies, while the young population of galaxies mainly reside in smaller halos. This segregation may be understood by the same mechanisms of anti-bias of galaxies at high density regions. As discussed in § 3.2, due to the suppression of galaxy formation in high temperature regions at lower redshift, and/or a different formation epoch for over- and under-dense regions, we have the deficiency of the young population of galaxies within massive dark halos at  $z = 0$ , and galaxies formed at high redshift trapped within the gravitational potential of dark halos gradually tend to trace the distribution of underlying dark matter.

The difference of the clustering amplitude can be also quantified by their two-point correlation functions at  $z = 0$  as plotted in Figure 14. The old population indeed clusters more strongly than the mass, and the young population is anti-biased. The relative bias between the two populations  $b_{\xi,g}^{\text{rel}} \equiv \sqrt{\xi_{\text{old}}/\xi_{\text{young}}}$  ranges 1.5 and 2 for  $1h^{-1}\text{Mpc} < r < 20h^{-1}\text{Mpc}$ , where  $\xi_{\text{young}}$  and  $\xi_{\text{old}}$  are the two-point correlation functions of the young and old populations. Again this is completely consistent with the observational indications that the clustering of early-type galaxies is stronger than that of late-type galaxies by a factor of 3–4 in terms of the amplitude of two-point correlation functions (Loveday et al. 1995; Hermit et al. 1996).

All the above results suggest that the old and young populations of galaxies in our simulations may be interpreted as the early-type and late-type galaxies in the present universe, and that the formation epoch and the hydrodynamical environment play the important role in determining the morphology of galaxies. We note here that the above result is fully consistent with the recent analysis of the IRAS PSCz galaxy sample by Jing, Börner, & Suto (2001), who found a strong anti-bias of the IRAS-selected galaxies (and thus mainly late-types). The degree of the detected bias is accounted for by the phenomenological cluster-underweight bias model (Jing, Mo & Börner 1998), and also by the semi-analytic modeling of galaxy formation which assumes that the galaxy morphology is determined by the frequency of the major merger of halos (Kauffmann, Chalrot & White 1996; Kauffmann, Nusser & Steinmetz 1997; Kauffmann et al. 1999).

## 5. CONCLUSIONS AND DISCUSSION

Using a cosmological SPH simulation, we directly simulate the formation of galaxies via radiative cooling of baryonic component and identify galaxies as isolated and distinct groups of cold gas particles. We calculated the biasing of galaxies and dark halos, and in particular, compared their properties with the theoretical prediction of the halo biasing model proposed by TS.

Our major findings are summarized as follows;

(1) The clustering of dark halos suffers from the the volume exclusion effect due to their finite size, especially at small scales. On the other hand, the halo biasing model by TS can reasonably account for the clustering of “galaxies” at large scales. At smaller scales, however, galaxies are anti-biased relative to dark matter at high density and thus high temperature environment.

(2) The biasing parameters are strongly time-dependent. At  $z \sim 3$ , our galaxies exhibit strong biasing;  $b_{\text{cov,g}} \simeq 3\text{--}4$  and  $b_{\xi,\text{g}} \simeq 3$ , which is consistent with the observed clustering of Lyman-break galaxies (Adelberger et al. 1998; Giavalisco et al. 1998; Steidel et al. 1998).

(3) The formation epoch  $z_f$  is the major parameter in determining the morphological type of galaxies. In our specific example, galaxies identified at  $z = 0$  with  $z_f > 1.7$  and  $z_f < 1.7$  can be roughly regarded as early-type and late-type galaxies, respectively. The former tightly correlates with the massive host halos and shows stronger clustering, while the latter is anti-biased and more stochastic. These suggest that biasing properties of galaxies, identified by different photometric bands or color selections, should be significantly different, which should be kept in mind in comparing the galaxy clustering from different galaxy catalogues.

Our current definition of galaxies in simulation data is admittedly rather phenomenological. Apparently more observationally oriented classification of galaxies, for example using color or magnitude of galaxies, is necessary for direct comparison with observations. We plan to implement more realistic prescriptions of galaxy formation and evolution including star formation, feedback and UV background heating in due course. Nevertheless it is quite encouraging that even a simple scheme described here explains the major properties of galaxy clustering in the universe.

We thank an anonymous referee for many useful comments, in particular for important comments on the dependence of galaxy biasing on their formation epoch and the importance of the artificial overmerging effect in the current simulations. We also thank S. Gottlöber for a careful reading of the manuscript. K.Y. and A.T. gratefully acknowledge support from JSPS (Japan Society for the Promotion of Science) fellowships. Y.P.J. is supported in part by the One-Hundred-Talent Program, by NKBRF (G19990754) and by NSFC. Numerical computations were carried out at ADAC (the Astronomical Data Analysis Center) of the National Astronomical Observatory, Japan and at KEK (High Energy Accelerator Research Organization, Japan). This research was supported in part by the Grant-in-Aid by the Ministry of Education, Science, Sports and Culture of Japan (07CE2002, 12640231), and by the Supercomputer Project (No.99-52, No.00-63) of KEK.

## REFERENCES

- Adelberger, K.L., Steidel, C.C., Giavalisco, M., Dickinson, M., Pettini, M. & Kellogg, M. 1998, ApJ, 505, 18
- Bagla, J.S. 1998, MNRAS, 299, 417
- Benson, A.J., Cole, S., Frenk, C.S., Baugh, C.M., & Lacey, C.G. 2000, MNRAS, 311, 793
- Benson, A.J., Pearce, F.R., Frenk, C.S., Baugh, C.M. & Jenkins, A. 2001, MNRAS, 320, 261
- Bertschinger, E. 1995, astro-ph/9506070
- Blanton, M., Cen R., Ostriker, J.P. & Strauss, M.A. 1999, ApJ, 522, 590
- Blanton, M., Cen, R., Ostriker, J.P., Strauss, M.A. & Tegmark, M. 2000, ApJ, 531, 1
- Bond, J.R., Cole, S., Efstathiou, G. & Kaiser, N. 1991, ApJ, 379, 440
- Bunn, E.F., & White, M. 1997, ApJ, 480, 6
- Cen, R., & Ostriker, J.P. 2000, ApJ, 538, 83
- Colín, P., Klypin, A., Kratsov, A., & Khokhlov, A. 1999, ApJ, 523, 32
- Copi, C.J., Schramm, D.N. & Turner, M.S. 1995, ApJ, 455, 95
- Davis, M., Efstathiou, G., Frenk, C.S. & White, S.D.M. 1985, ApJ, 292, 371
- Dekel, A. & Lahav, O. 1999, ApJ, 520, 24
- Dressler, A. 1980, ApJ, 236, 351
- Dressler, A., Oemler, A., Couch, W.J., Smail, I., Ellis, R.S., Barger, A., Butcher, H., & Poggianti, B.M. 1997, ApJ, 490, 577
- Eisenstein, D. & Hut, P., 1998, ApJ, 498, 137
- Fry, J. 1996, ApJ, 461, 65
- Fukugita, M., Hogan C.J. & Peebles, P.J.E. 1998, ApJ, 503, 518
- Gelb, J.M., & Bertschinger, E. 1994, ApJ, 436, 467
- Giavalisco, M., Steidel, C.C., Adelberger, K.L., Dickinson, M.E., Pettini, M., & Kellogg, M. 1998, ApJ, 503, 543
- Gottlöber, S., Klypin, A.A., & Kravtsov, A.V. 1999, in the proceedings of the MPA- ESO cosmology conference, “Evolution of large scale structure : from recombination to Garching” (Garching, ESO), edited by Banday, A.J., Sheth, R.K., & da Costa, L.N. p.358

- Hamana, T., Colombi, S., & Suto, Y. 2001, *A&A*, 367, 18
- Hamilton, A.J.S., Kumar, P., Edward, Lu. & Matthews, A. 1991, *ApJL*, 374, L1
- Hermit, S., Santiago, B.X., Lahav, O., Strauss, M.A., Davis, M., Dressler, A. & Huchra, J. P. 1996, *MNRAS*, 283, 709
- Hikage, C., Taruya, A., & Suto, Y., *ApJ*, 556 August 1 issue, in press (astro-ph/0104013)
- Hockney, R.W. & Eastwood, J.W. 1981, *Computer Simulation Using Particles* (New York: McGraw Hill)
- Jenkins, A., Frenk, C.S., White, S.D.M., Colberg, J.M., Cole, S., Evrard, A.E. & Yoshida, N. 2001, *MNRAS*, 321, 372
- Jing, Y.P. 1998, *ApJ*, 503, L9
- Jing, Y.P., Börner, G., & Suto, Y. 2001, *ApJ*, submitted (astro-ph/0104023)
- Jing, Y.P., Mo, H.J., & Börner, G. 1998, *ApJ*, 494, 1
- Jing, Y.P. & Suto, Y. 1998, *ApJL*, 494, L5
- Kauffmann, G., Charlot, S., & White, S.D.M. 1996, *MNRAS*, 283, 117
- Kauffmann, G., Nusser, A., & Steinmetz, M. 1997, *MNRAS*, 286, 795
- Kauffmann, G., Colberg, J.M., Diaferio, A., & White, S.D.M. 1999, *MNRAS*, 307, 529
- Kennicutt, R.C. 1998, *ARA&A*, 36, 189
- Kitayama, T. & Suto, Y. 1996, *ApJ*, 469, 480
- Kitayama, T. & Suto, Y. 1997, *ApJ*, 490, 557
- Klypin, A.A., Gottlöbar, S., Kravtsov, A.V., & Khokhlov, A.M. 1999, *ApJ*, 516, 530
- Kravtsov, A.V. & Klypin, A.A. 1999, *ApJ*, 520, 437
- Loveday, J., Maddox, S.J., Efstathiou, G. & Peterson, B. A. 1995, *ApJ*, 442, 457
- Mo, H.J., & White, S.D.M 1996, *MNRAS*, 282, 347
- Navarro, J., Frenk, C. & White, S.D.M. 1997, *ApJ*, 490, 493
- Pearce, F.R., Jenkins, A., Frenk, C.S., Colberg, J.M., White, S.D.M., Thomas, P.A., Couchman, H.M.P., Peacock, J.A. & Efstathiou, G. 1999, *ApJL*, 521, L99
- Peacock, J.A. & Dodds, S.J. 1996, *MNRAS*, 280, L19

- Postman, M. & Gellar, M. 1984, *ApJ*, 281, 95
- Press, W.H. & Schechter, P. 1974, *ApJ*, 187, 425
- Roberts, M.S., & Haynes, M. 1994, *ARA&A*, 32, 115
- Somerville, R.S., Lemson, G., Sigrad, Y., Dekel, A., Kauffmann, G. & White, S.D.M. 2000, *MNRAS*, 320, 289
- Springel, V., White, S.D.M., Tormen, G., & Kauffmann, G. 2000, submitted to *MNRAS* (astro-ph/0012055)
- Steidel, C.C., Adelberger, K.L., Dickinson, M., Giavalisco, M., Pettini, M. & Kellogg, M. 1998, *ApJ*, 492, 428
- Sutherland, R.S. & Dopita, M.A. 1993, *ApJS*, 88, 253
- Suto, Y. 1993, *Prog.Theor.Phys.* 90, 117
- Suto, Y., Magira, H., Jing, Y.P., Matsubara, T. & Yamamoto, K. 1999, *Prog.Theor.Phys.Suppl.* 133, 183
- Suto, Y., Magira, H., & Yamamoto, K. 2000, *PASJ* 52, 249
- Taruya, A. & Suto, Y. 2000, *ApJ*, 542, 559 (TS)
- Taruya, A., Magira, H., Jing, Y.P., & Suto, Y. 2001, *PASJ*, 53 , in press
- Tegmark, M. & Peebles, P.J.E. 1998, *ApJ*, 500,79
- Tegmark, M. & Bromley, B.C. 1999, *ApJL*, 518, 69
- Thacker, R.J., Tittley, E.R., Pearce, F.R., Couchman, H.M.P. & Thomas, P.A. 2000, *MNRAS*, 319, 619
- Yoshikawa, K., Jing, Y.P. & Suto, Y. 2000, *ApJ*, 535, 593



Table 1. Number and mass range of identified objects and adopted linking length for FOF algorithm.

redshift	dark halo	galaxy	DM core
0.0	1797 (0.164 $\bar{l}$ ) $10^{12} M_{\odot} \sim 8.6 \times 10^{14} M_{\odot}$	1604 (0.0164 $\bar{l}$ ) $10^{11} M_{\odot} \sim 9.5 \times 10^{12} M_{\odot}$	1525 (0.05 $\bar{l}$ ) $4.3 \times 10^{11} M_{\odot} \sim 2.0 \times 10^{14} M_{\odot}$
0.5	2105 (0.184 $\bar{l}$ ) $10^{12} M_{\odot} \sim 3.5 \times 10^{14} M_{\odot}$	1936 (0.0246 $\bar{l}$ ) $10^{11} M_{\odot} \sim 6.8 \times 10^{12} M_{\odot}$	1721 (0.05 $\bar{l}$ ) $4.3 \times 10^{11} M_{\odot} \sim 6.3 \times 10^{13} M_{\odot}$
1.0	2201 (0.192 $\bar{l}$ ) $10^{12} M_{\odot} \sim 2.3 \times 10^{14} M_{\odot}$	1861 (0.0328 $\bar{l}$ ) $10^{11} M_{\odot} \sim 3.6 \times 10^{12} M_{\odot}$	1543 (0.05 $\bar{l}$ ) $4.3 \times 10^{11} M_{\odot} \sim 2.9 \times 10^{13} M_{\odot}$
2.0	1859 (0.197 $\bar{l}$ ) $10^{12} M_{\odot} \sim 8.2 \times 10^{13} M_{\odot}$	1360 (0.0492 $\bar{l}$ ) $10^{11} M_{\odot} \sim 2.0 \times 10^{12} M_{\odot}$	765 (0.05 $\bar{l}$ ) $4.3 \times 10^{11} M_{\odot} \sim 9.8 \times 10^{12} M_{\odot}$
3.0	1165 (0.199 $\bar{l}$ ) $10^{12} M_{\odot} \sim 3.8 \times 10^{13} M_{\odot}$	996 (0.0656 $\bar{l}$ ) $10^{11} M_{\odot} \sim 1.4 \times 10^{12} M_{\odot}$	278 (0.05 $\bar{l}$ ) $4.3 \times 10^{11} M_{\odot} \sim 4.2 \times 10^{12} M_{\odot}$

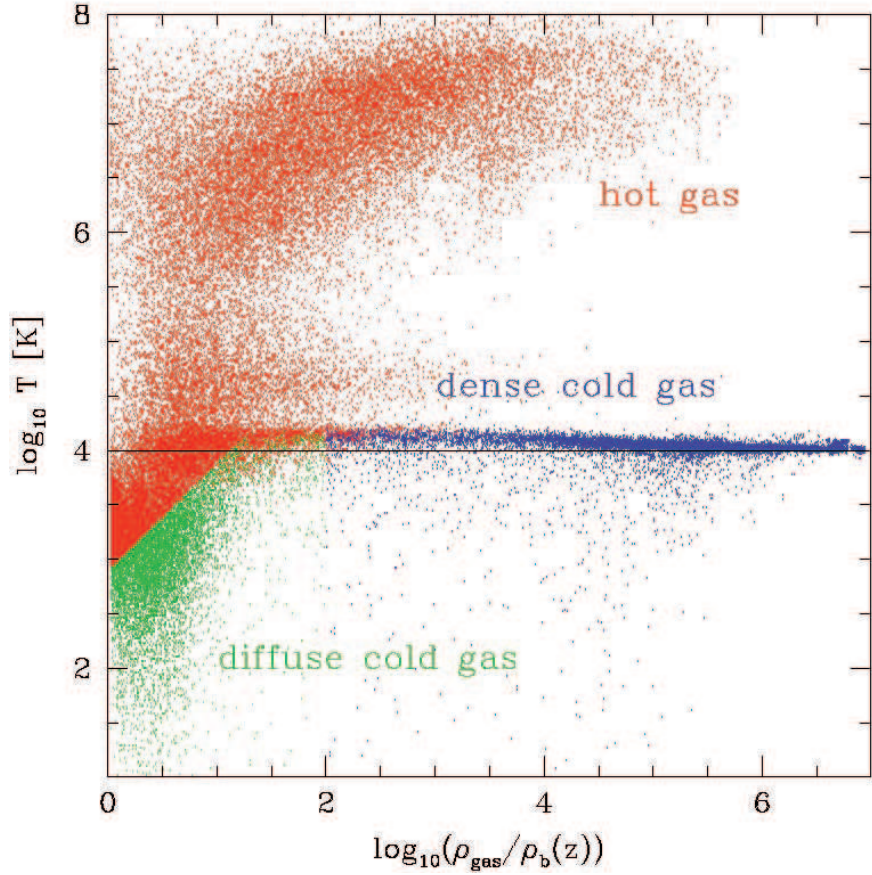


Fig. 1.— Scatter plot of gas particles at  $z = 0$  in  $\log \rho_{\text{gas}}\text{-}\log T$  plane. The cold and dense gas particles which satisfy the criterion (1) and  $\rho_{\text{gas}} > 10^2 \bar{\rho}_{\text{b}}(z)$  are indicated by blue points, the diffuse cold gas with  $\rho_{\text{gas}} > 10^2 \bar{\rho}_{\text{b}}(z)$  are by green points and the others are by red points.

Fig. 2.— Distribution of gas particles, dark matter particles, galaxies and dark halos in the volume of  $75h^{-1} \times 75h^{-1} \times 30h^{-1}\text{Mpc}^3$  model at  $z = 0$ . *Upper-right*: gas particles; *Upper-left*: dark matter particles; *Lower-right*: galaxies; *Lower-left*: DM cores

Fig. 3.— Same as Figure 2 but for  $z = 2$ .

Fig. 4.— Snapshots of the most massive cluster ( $M \simeq 8 \times 10^{14}M_{\odot}$ ) in the simulation at  $z = 0$ . *Upperleft*: dark matter; *Upper-right*: gas; *Lower-left*: DM cores; *Lower-right*: cold gas. Circles in lower panels indicate the positions of galaxies identified according to our criteria. The comoving size of the box is  $6.25h^{-1}\text{Mpc}$  per side.

Fig. 5.— Same as Figure 4 but for a poorer cluster with  $M \simeq 10^{14}M_{\odot}$ .

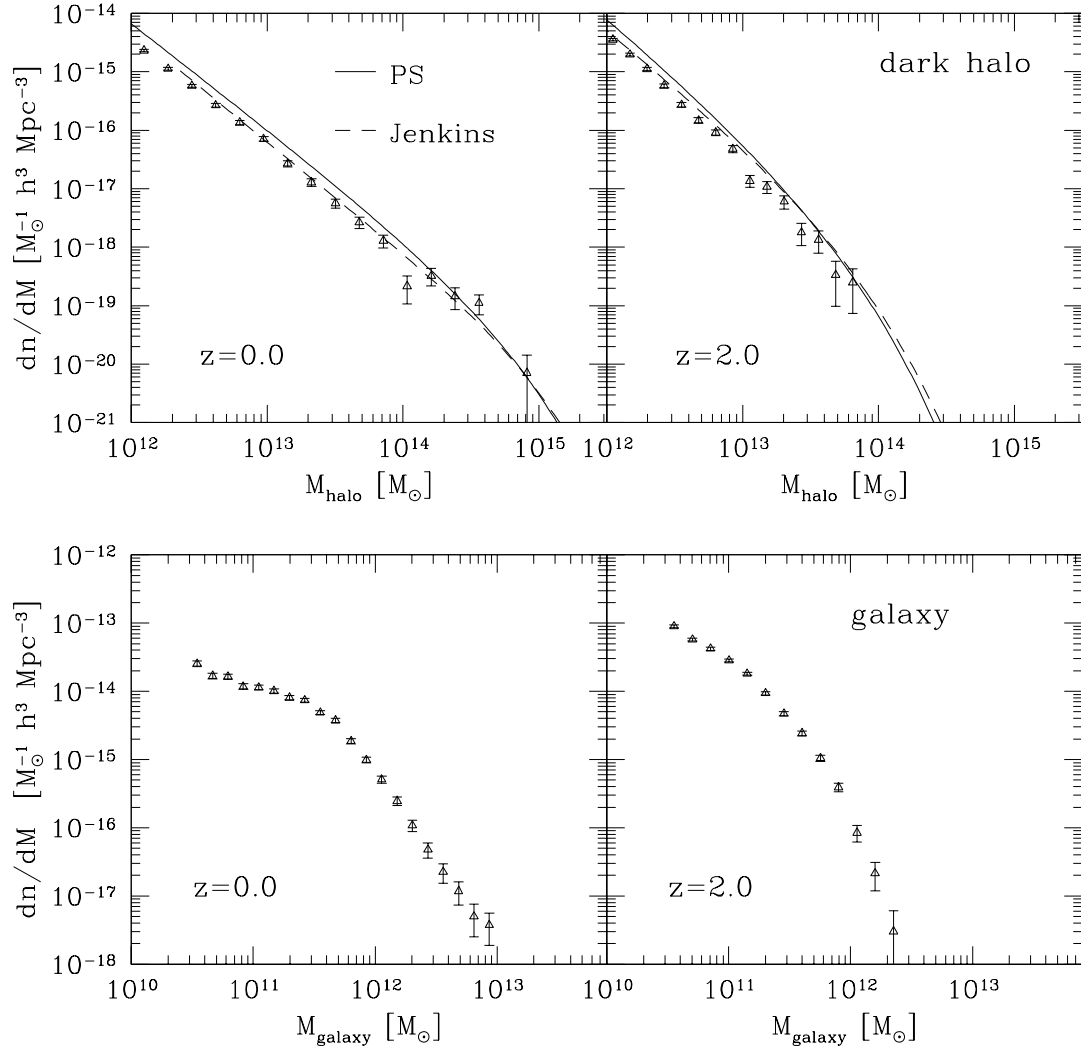


Fig. 6.— Mass functions of dark halos and galaxies at redshift  $z = 0$  and  $z = 2$ . Solid lines in upper panels are theoretical predictions of Press–Schechter mass function and dashed lines are fitting formula by Jenkins et al. (2001).

Fig. 7.— Joint probability distributions of overdensity fields for dark halos and galaxies with dark matter overdensity smoothed over  $R_s = 12h^{-1}\text{Mpc}$  (*Upper panels*) and  $R_s = 4h^{-1}\text{Mpc}$  (*Lower panels*) at redshift  $z = 0, 1$  and  $2$ . Solid lines indicate the conditional mean  $\bar{\delta}_i(\delta_m)$  for each object. Dashed lines in each panel depict the theoretical prediction of conditional mean by Taruya & Suto (2000).

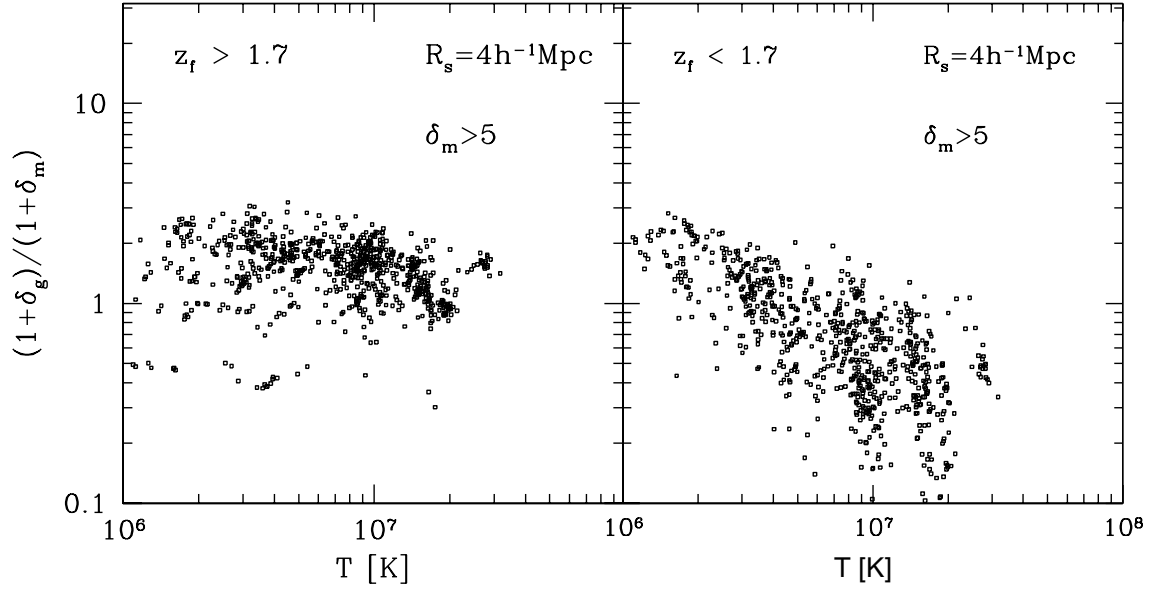


Fig. 8.— Relation between environmental temperature and the ratios of dark matter overdensity with that of galaxies with  $z_f > 1.7$  (*left panel*) and  $z_f < 1.7$  (*right panel*) in the high density regions ( $\delta_m > 5$ ). Each point corresponds to the randomly selected point in the simulation box. The smoothing scale is set to  $R_s = 4h^{-1}\text{Mpc}$ .

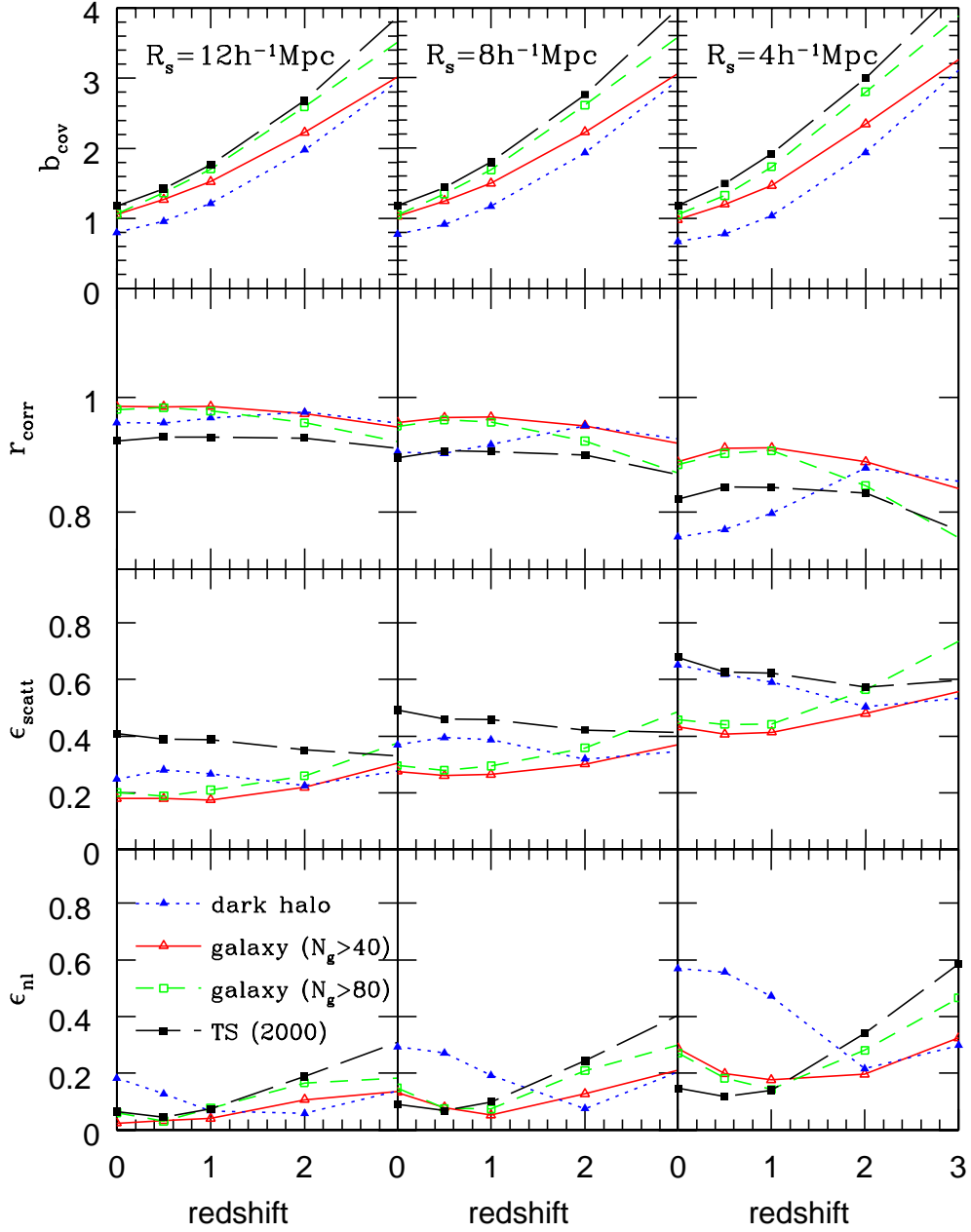


Fig. 9.— Evolution of biasing parameters  $b_{\text{cov}}$ ,  $r_{\text{corr}}$ ,  $\epsilon_{\text{scatt}}$  and  $\epsilon_{\text{nl}}$  for galaxies (solid lines), dark halos (dotted lines), and the theoretical predictions by Taruya & Suto (2000) (long dashed lines).

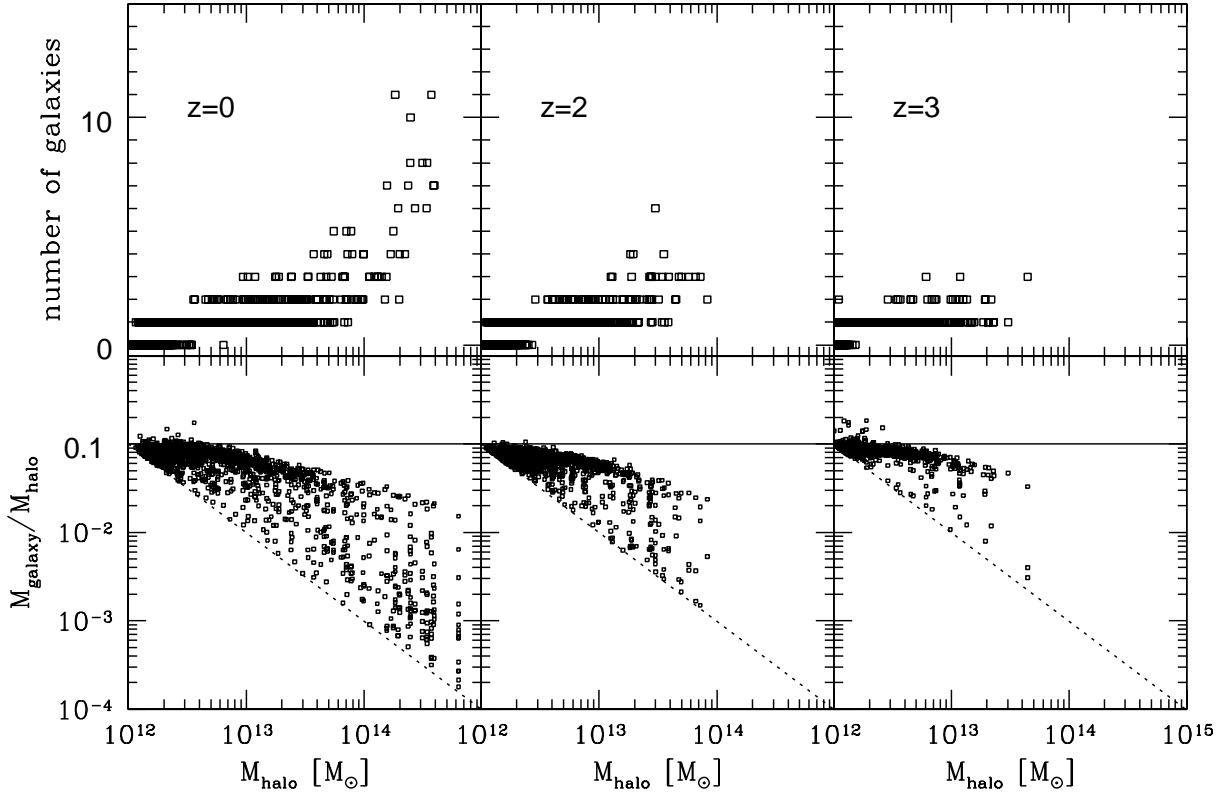


Fig. 10.— Number of galaxies which reside in a dark halo (*upper panels*) and distributions of mass ratio between galaxies and dark halos which host them (*lower panels*) at redshift  $z = 0$  and 2. Solid and dashed lines in lower panels indicate the mean baryon fraction ( $\Omega_b/\Omega_0$ ) and resolution limit constrained by the minimum mass of galaxies in their definition (see §2.2), respectively.



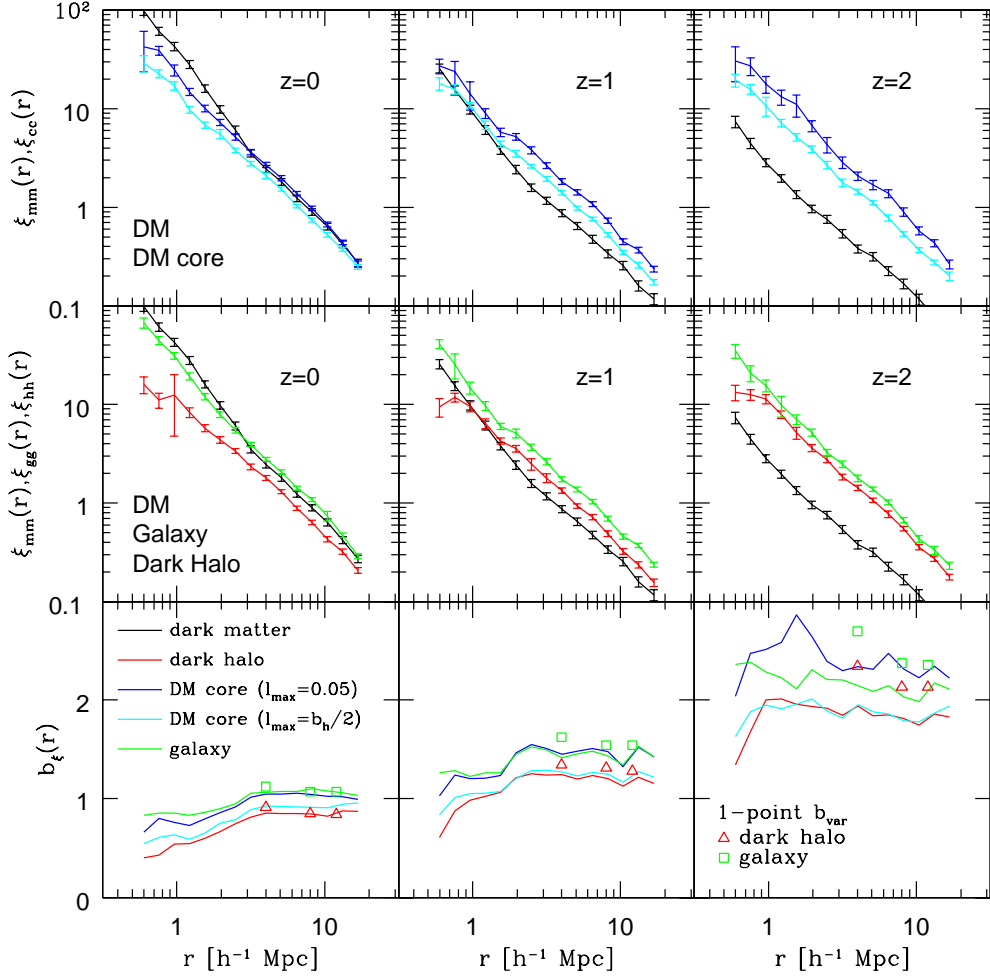


Fig. 11.— Upper panels show two-point correlation functions for dark matter and DM cores at redshift  $z = 0, 1$  and  $2$ . Middle panels for those of dark matter, galaxies and dark halos. In lower panels, the profiles of biasing parameter  $b_{\xi}(r)$  for dark halos, DM cores and galaxies at  $z = 0.0, 1$  and  $2$  are shown. In lower panels, we also plot the parameter  $b_{\text{var}}$  on the smoothing scale  $R_s = 4h^{-1}\text{Mpc}, 8h^{-1}\text{Mpc}$  and  $12h^{-1}\text{Mpc}$  at  $r = R_s$  for each kind of objects by different symbols.

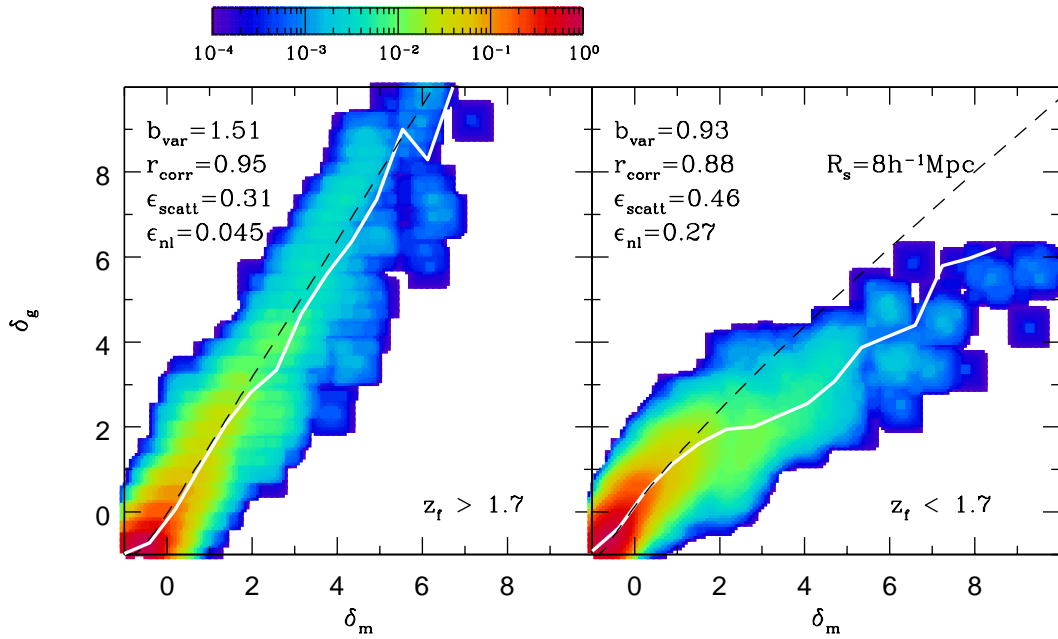


Fig. 12.— Joint probability distributions of density fields of dark matter and galaxies with different formation epochs on the scale of  $R_s = 8h^{-1}\text{Mpc}$ . Left panel is for galaxies with  $z_f > 1.7$  and right panel for ones with  $z_f < 1.7$ . Solid lines indicate the simulated mean relations. For comparison, the predictions of mean biasing for dark halos with their formation redshift greater and less than 1.7. are shown in left and right panels, respectively.

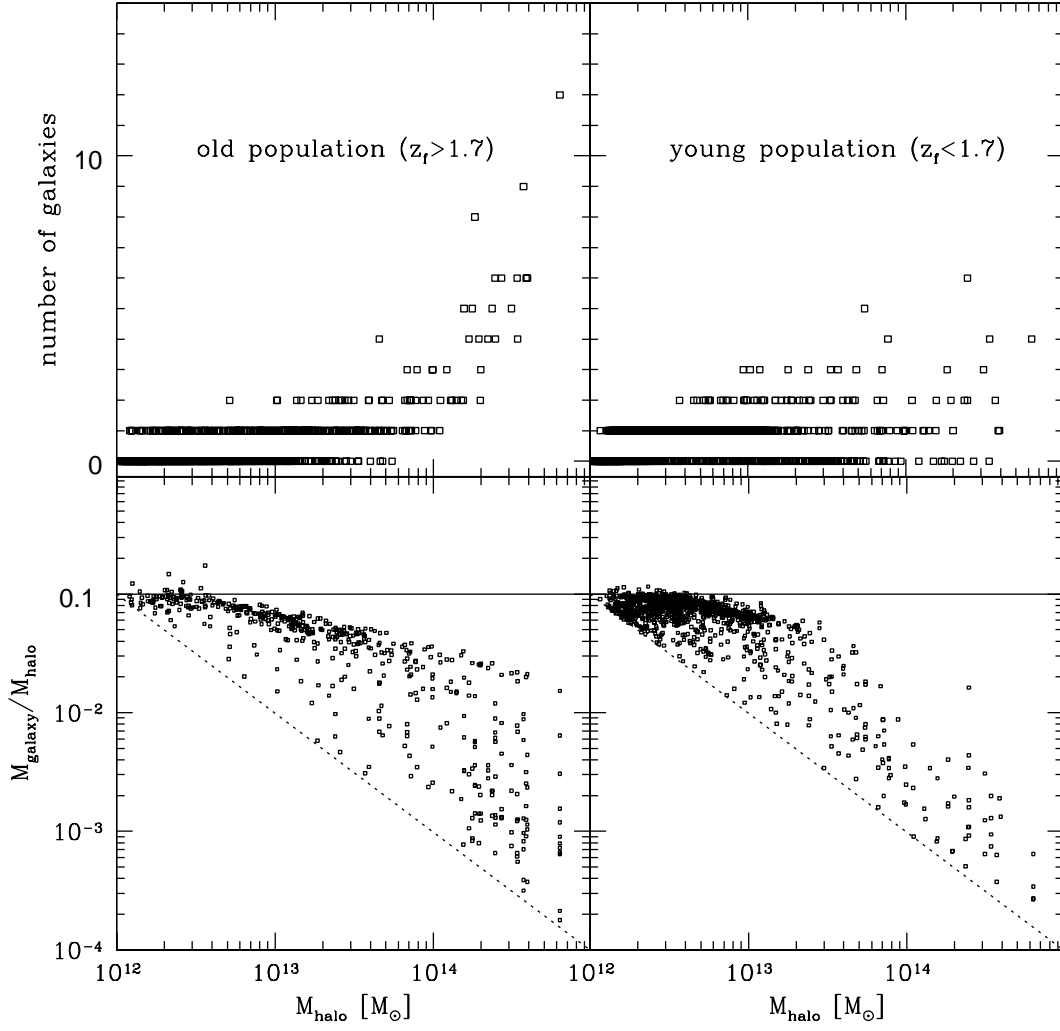


Fig. 13.— Same as Figure 10 except for old (*left*) and young (*right*) populations of galaxies at  $z = 0$ .

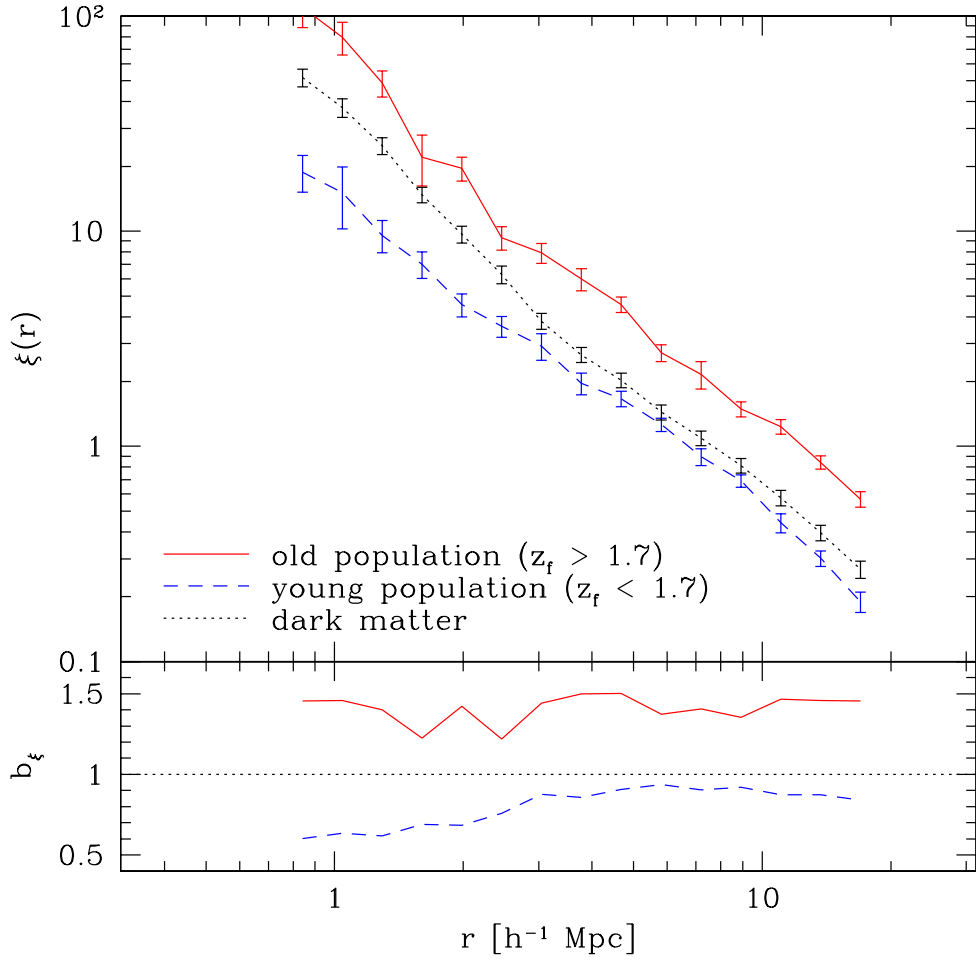


Fig. 14.— Two-point correlation functions for the old and young populations of galaxies at  $z = 0$  as well as that of dark matter distribution. The profiles of bias parameters  $b_\xi(r)$  for both of the two populations are also shown in the lower panel.

This figure "f2.jpg" is available in "jpg" format from:

<http://arxiv.org/ps/astro-ph/0104361v1>

This figure "f3.jpg" is available in "jpg" format from:

<http://arxiv.org/ps/astro-ph/0104361v1>

This figure "f4.jpg" is available in "jpg" format from:

<http://arxiv.org/ps/astro-ph/0104361v1>

This figure "f5.jpg" is available in "jpg" format from:

<http://arxiv.org/ps/astro-ph/0104361v1>



This figure "f7a.jpg" is available in "jpg" format from:

<http://arxiv.org/ps/astro-ph/0104361v1>

This figure "f7b.jpg" is available in "jpg" format from:

<http://arxiv.org/ps/astro-ph/0104361v1>